Mansoura Engineering Journal

Volume 20 | Issue 1 Article 6

3-1-2020

# Effect of Magnetic Flux Fringing at Pole Edges on Parameters and Performance of E-Core Heteropolar Linear Synchronous Motor.

S. El-Drieny
*Assistant Professor of Electrical Engineering Department, Faculty of Engineering, El-Mansoura University, El-Mansoura, Egypt.*

# EFFECT OF MAGNETIC FLUX FRINGING AT POLE EDGES ON PARAMETERS AND PERFORMANCE OF E-CORE HETEROPOLAR LINEAR SYNCHRONOUS MOTOR

## تأثير تهدب الفيض المغناطيسى عند أحرف القطب على ثوابت وأداء المحرك التزامنى الخطى غير متجانس الاقطاب ذو القلب الحديدى على شكل E

Dr. S. A. El-Drieny
Electrical Engineering Department,
Faculty of Engineering, El-Mansoura University,
El-Mansoura, Egypt

**ملخص البحث**

المحرك التزامنى الخطى ذو القلب الحديدى - E هو أحدث محرك فى مجموعة المحركات الخطية القادرة على إحداث كل من قوتى الرفع والجر الكهربى. ونظرا لطبيعة تكوين الدوائر المغناطيسية المكافئة الناتجة عن مثل هذا الشكل الهندسى للقلب الحديدى والتى تختلف طبقا لمصادر القوة الدافعة المغناطيسية فى إتجاه محور القطب والمحور المتعامد، فإنه يجب بذل عناية خاصة عند حساب ثوابت الآله ($M_{af}$, $L_f$, $L_{ad}$, $L_{aq}$) حيث يتوقف عليها الأداء المتوقع للمحرك خاصه قوتى الرفع والجر الكهربى. يهتم هذا البحث بحساب ثوابت الآله تحت تأثير "ظاهرة التهدب المغناطيسى" الناشىء عند أحرف الأقطاب، حيث تؤثر تلك الظاهرة على قيم الممانعة التى يلاقيها الفيض المغناطيسى فى الثغرة الهوائية أثناء عبوره للقائم الأوسط والقائمين الخارجين، وتتوقف هذه الممانعه على "المساحة الفعالة للقطب" والذى يمتد من تحت القائم الخارجى حتى القائم الأوسط للقلب الحديدى، وهذه "المساحة الفعالة" للقطب تتوقف بدورها على "العرض الفعال" له والذى يزداد فى القيمة عن العرض الهندسى بالقدر الذى يتناسب مع تأثير التهدب المغناطيسى الحادث. هذه الزيادة فى عرض القطب تعتمد على طول الثغرة الهوائية، عرض السنة، عمق القطب. وأيضا تختلف بطبيعة مسار الفيض المغناطيسى والذى يتمثل فى : (١) فيض مغناطيسى متعامد على اتجاه حركة المحرك والناشىء عن القوة الدافعة المغناطيسية لملفات التيار المستمر ومركبة القوة الدافعة المغناطيسية لملفات التيار المتردد فى إتجاه محور القطب. (٢) فيض مغناطيسى موازى لإتجاه حركة المحرك والناشىء عن مركبة القوة الدافعة المغناطيسية لملفات التيار المتردد فى إتجاه عمودى على محور القطب. بإستنتاج العلاقات اللازمة لإيجاد الأبعاد الفعالة للقطب تحت تأثير التهدب المغناطيسى يمكن إيجاد قيم الممانعة فى الثغرة الهوائية وقيم الفيض المغناطيسى فى إتجاه محور القطب والمحور المتعامد. وإستنتاج العلاقات اللازمة لحساب ثوابت الآلة، ومن ثم يتمكن المصمم بطريقه سهلة وسريعة من حساب الأداء المتوقع للمحرك خاصة قوتى الرفع والجر الكهربى بدرجة ملحوظة من الدقة. وللتدليل على دقة الأسلوب الذى اتبع فى حساب ثوابت الآلة تحت تأثير التهدب المغناطيسى تم بناء "نموذج إستاتيكى" للآلة تم عليه قياس القوة الدافعة الكهربية المستنتجة فى ملفات التيار المتردد من خلال قياس قيمة الفيض المغناطيسى المتوسطة فى الثغرة الهوائية وتم مقارنة النتائج المعملية بالنتائج المحسوبة تحت تأثير ظاهرة التهدب المغناطيسى وبدونه، وقد أظهرت النتائج تقاربا ملحوظا للقيم المحسوبة تحت تأثير ظاهرة التهدب المغناطيسى مع تلك التى تم قياسها على النموذج.

## ABSTRACT

Recently, the E-core linear synchronous motor has been introduced to the family of linear motors capable of exerting both traction and attraction forces. Due to the complexity of the magnetic structure of such core-shape, attention must be paid while evaluating the machine parameters. Thereby, more exact estimation of the expected machine performance can be ensured.

This paper is concerned mainly with the proper evaluation of the parameters of the E-core linear synchronous motor; taking into consideration the flux fringing effect. This effect is one of the most important factors which influence the air-gap reluctance faced by both the transverse and tangitudinal fluxes. The developed approach to simulate the flux fringing in the air-gap regions has been resulted in a simple way to get the effective pole areas under the middle and outer limbs. Accordingly, the values of center air-gap permeance

corresponding to different air-gap flux components ($\phi_f$, $\phi_{ad}$, $\phi_{aq}$) and intern the machine parameters ($M_{af}$, $L_f$, $L_{ad}$, $L_{aq}$) can be exactly evaluated. This way, the machine performance, especially the traction and attraction forces, can be properly and easily predicted at this phase of motor design process.

Experimental measurements are carried out on a simple static model to verify the proposed approach. The comparison between the theoretical results, considering effect of magnetic flux fringing at pole edges, and experimental results on a static prototype motor shows that they are in a good agreement.

## 1. INTRODUCTION :

Linear motors with transverse magnetic circuit providing both traction and attraction forces were introduced in 1972 [1] A recent addition to this class of linear motors is the E-core type [2] and it is shown in Fig. (1). Several complicated magnetic circuits are established in this machine due to its core shape and the type of MMF along a given magnetic axis. Therefore attention must be paid during the estimation process of the parameters of this motor. If these parameters are not exactly estimated, the traction force required will not match with the required attraction force. This paper is concerned with the parameters evaluation of the E-core linear synchronous motor ; taking into account the phenomena of flux fringing at pole edges. This phenomena affects the air-gap permeance under the middle and outer core limbs. Accordingly, the air-gap permeances are influenced by both the type of excitation (DC and AC excitation) and the effective pole area. The total flux along the d-axis, due to the DC excitation and the corresponding component of the AC excitation, crosses the central air-gap in a direction normal to the motion. Similarly, the flux along the q-axis, due to the corresponding component of the AC excitation, crosses the central air-gap in a direction tangential to the motion. Regarding the pole area, there are two effective pole areas, one under the middle core limb and the other under the outer core limb. The effective pole area is greater than the geometric pole area by an amount sufficient to compensate the fringing magnetic flux at pole edges. For a given dimension of E-core especially the widths of middle and outer limbs, the effective pole area depends on the pole width. The increased amount of pole width depends on : air-gap, tooth width and pole depth . Once the effective pole areas under the middle and outer core limbs have been estimated ,considering the effect of magnetic flux fringing at pole edges, the air-gap permeances , the flux components , the inductances, the attraction and traction forces were estimated.

The given approach depends on the assumption of neglecting end-loss, saturation in all iron parts, all flux leakage and all harmonics in MMF produced by AC and DC windings. To verify the given approach an experimental tests were carried out on a prototype static motor. This prototype was built in electric machine laboratory , El mansoura University. The induced e.m.f was measured in A.C windings using the average value of the flux at pole pitch . The comparison between experimental results and theoretical one inclusive effect of magnetic flux fringing at pole edges show that they are more close together.

## 2. Air-gap Permeance :

To get the centre air-gap permeance $S_1$ assuming the corresponding flux paths to follow circular fringes outside the gap as indicated in Fig.(2a & 2b), and the air-gap, g, is multiplied by Carter's

coefficient to allow for slotting of the stator. In accordance with $S_2$, the outside air-gap permeance, the division of flux paths is similar to that of $S_1$.

The flux carrying region can be divided into seven individual regions possessing the following permeances [6].

| Centre gap $S_1$ | Outside gap $S_2$ |
|---|---|
| $s_1' = \mu_o w_1 l_1 / g'$ | $s_1 = \mu_o w_2 l_2 / g$ |
| $s_2' = 0.610\ \mu_o l_1$ | $s_2 = 0.610\ \mu_o l_2$ |
| $s_3' = 0.305\ \mu_o l_1$ | $s_3 = 0.305\ \mu_o l_2$ |
| $s_4' = (\mu_o l_1 / \pi).\ln(1+2h/g')$ | $s_4 = (\mu_o l_2 / \pi).\ln(1+2h/g)$ |
| $s_5' = (2\mu_o l_1 / \pi).\ln(1+h/g')$ | $s_5 = (2\mu_o l_2 / \pi).\ln(1+h/g)$ |
| $s_6' = 0.610\ \mu_o w_1$ | $s_6 = 0.610\ \mu_o w_2$ |
| $s_7' = (2\mu_o w_1 / \pi).\ln(1+h/g')$ | $s_7 = (2\mu_o w_2 / \pi).\ln(1+h/g)$ |
| $S_1 = s_1'+s_2'+s_3'+s_4'+s_5'+2(s_6'+s_7')$ | $S_2 = s_1+s_2+s_3+s_4+s_5+2(s_6+s_7)$ |

$$S_1 = \mu_o . A_{1eff} / g' = s_1'+s_2'+s_3'+s_4'+s_5'+2(s_6'+s_7') \quad (1)$$

$$A_{1eff} = \frac{4w_1 g'}{\pi} \ln(1+h/g') + \frac{l_1 g'}{\pi} \ln(1+2h/g') + \frac{2l_1 g'}{\pi} \ln(1+h/g') + $$

$$+1.32 g' w_1 + w_1 l_1 + 0.915\ g' l_1 \quad (2)$$

Consequently the increased amount area under centre air-gap is given by:

$$\Delta a_1 = A_{1eff} - w_1 l_1 = \frac{4w_1 g'}{\pi} \ln(1+h/g') + \frac{l_1 g'}{\pi} \ln(1+2h/g') + \frac{2l_1 g'}{\pi} \ln(1+h/g') +$$

$$+1.32 g' w_1 + 0.915\ g' l_1 \quad (3)$$

In similar the increased amount area under outer air-gap is given by :

$$\Delta a_2 = \frac{4w_2 g}{\pi} \ln(1+h/g) + \frac{l_2 g}{\pi} \ln(1+2h/g) + \frac{2l_2 g}{\pi} \ln(1+h/g) +$$

$$+1.32 g w_2 + 0.915\ g l_2 \quad (4)$$

## 3. Prediction of Performance Characteristics :

### 3.1. Field Winding Mutual and Self Inductances ($M_{af}$ and $L_f$) :

The field flux takes a transverse paths Fig.(1) , crossing a two air-gaps in each pole pitch and giving a flux density under the centre limb as following:

$$2Z_f I_f = H_1 g + H_2 g$$

$$2Z_f I_f = (g/\mu_o)(B_{1f} + B_2) \qquad (5)$$

$$\phi = B_{1f} A_1 = B_2 A_2 \quad \text{assuming zero pole leakage.}$$

$$= B_{1f} w_1 l_{id} = B_2 w_2 l_2$$

$$B_2 = B_{1f} (w_1 l_{id} / w_2 l_2) \qquad (6)$$

from (1) and (2)

$$B_{1f} = (2\mu_o Z_f I_f)/[g(1 + (w_1 l_{id}/w_2 l_2))] \qquad (7)$$

The total flux per pole is equal to the average flux density over the whole pole width multiplied by the air-gap area ($\tau_p . w_1$) , where ;

$$\phi_f = (w_1 . \tau_p) . ((4B_{1f}/\pi^2) . \sin(\frac{\pi}{2} . \frac{l_{id}}{\tau_p})) \qquad (8)$$

and,

$$\phi_f = (w_1 . \tau_p) . (8/\pi^2) . [(\mu_o . Z_f . I_f)/\{g(1+(w_1 l_{id})/(w_2 l_2))\}] . \sin(\frac{\pi}{2} . \frac{l_{id}}{\tau_p}) \qquad (9)$$

The induced RMS phase voltage can be expressed in terms of a mutual inductance or a rate of change of flux, i.e.,

$$M_{af} . I_f = 2(1/\sqrt{2}) . (Z_a . q . K_w . p) . \phi_f \qquad (10)$$

Substituting for $\phi_f$ from equation (8) into equation (10) gives the mutual inductance linking the field and armature windings.

$$M_{af} = \frac{8\sqrt{2} . w_1 . \tau_p . \mu_o . Z_f . p(Z_a . q . K_w)}{\pi^2 . g . (1+(w_1 . l_{id})/(w_2 . l_2))} . \sin(\frac{\pi}{2} . \frac{l_{id}}{\tau_p}) \qquad (11)$$

The instantaneous voltage induced in the field winding can be expressed in terms of a self inductance or a rate of change of flux. Since the field winding consists of two series connected sections, the voltage is given by ;

$$L_f . \frac{dI_f}{dt} = 2 . Z_f . p . \frac{d\phi_f}{dt}$$

Using equations (7) , (8) gives the field winding self inductance

$$L_f \cdot \frac{B_{if} \cdot g \cdot (1+(w_i l_{id}/w_2 l_2))}{\mu_o \cdot Z_f} = 2Z_f \cdot p \cdot \frac{8B_{if}}{\pi^2} \cdot w_i \cdot \tau_p \cdot \sin\left(\frac{\pi}{2} \cdot \frac{l_{id}}{\tau_p}\right)$$

then,

$$L_f = \frac{16\,\mu_o \cdot Z_f^2 \cdot p \cdot w_i \cdot \tau_p}{\pi^2 \cdot g \cdot (1+(w_i l_{id}/w_2 l_2))} \cdot \sin\left(\frac{\pi}{2} \cdot \frac{l_{id}}{\tau_p}\right) \qquad (12)$$

### 3.2. Armature q-axis Self Inductance $L_{aq}$ :

The q-axis field takes longitudinal paths [3] ,see Fig.(1), through the pole and the primary core. This flux component tends to emerge from the points on the armature winding at highest potential and these are furthest from the poles. The paths are almost entirely axial . Since the q-axis mmf component of armature winding at any point x from the centre pole along the machine length is given as [5]:

$$F_{aq}(x) = \hat{F}_a \sin(\pi x / \tau_p) \qquad 0 \le x \le \tau_p \qquad (13)$$

hence;

$$\phi_{q_1} = 2 \cdot \mu_o \cdot \frac{w_i}{g} \cdot \hat{F}_a \int_0^{+l_{iq}/2} \sin\left(\frac{\pi x}{\tau_p}\right) \cdot dx \qquad (14)$$

$$\phi_{q_2} = 2\,\frac{\mu_o\, w_i}{g}\ \hat{F}_a \int_{l_{iq}/2}^{\tau_p/2} \frac{\sin \pi x/\tau_p}{(\pi/2)\cdot(2x - l_{iq}/2)} \cdot dx \qquad (15)$$

The q-axis flux $\phi_q$ is given by $\phi_{q_1} + \phi_{q_2}$

$$\phi_q = C_q \cdot \frac{6\cdot(Z_a \cdot q \cdot K_w)\cdot \mu_o \cdot w_i \cdot \tau_p \cdot I}{\sqrt{2}\cdot \pi^2 \cdot g} \qquad (16)$$

Where ;

$$C_q = \frac{l_{iq}}{\tau_p} - \frac{1}{\pi} \cdot \sin\left(\frac{\pi}{2} \cdot \frac{l_{iq}}{\tau_p}\right)$$

Equating the expressions for the induced e.m.f., $E_{aq}$ and the air-gap quadrature reactance voltage drop $X_q \cdot I_{aq}$ .

$$L_{aq} \cdot I = \frac{2\cdot(Z_a \cdot q \cdot K_w)}{\sqrt{2}} \cdot p \cdot \phi_q \qquad (17)$$

Hence ; armature quadrature inductance can be obtained .

$$L_{aq} = C_q \cdot \frac{6.(Z_a.q.K_w)^2 . \mu_o . w_i . \tau_p . p}{\pi^2 . g} \qquad (18)$$

### 3.3. Armature d-axis Self-inductance ($L_{ad}$) :

The flux created by the armature winding is divided into two flux components in both d and q axes. The d-axis armature field takes transverse paths [4] , as the main field created by the D.C. excitation , see Fig.(1) . So, the same technique used to predict the behaviour of the main field can be used to predict the d-axis armature field. This can be analyzed using a magnetic equivalent circuit similar to that of the D.C. excitation with slight difference. This difference is due to the existence of the A.C. excitation on the centre limb of the core.

As the A.C. winding is a distributed one, the corresponding source of m.m.f. is distributed sinusiodally along the direction of the machine length. The equivalent m.m.f. in the direct axis , $F_{od}$ , is calculated by summing the flux contributions from each element under the centre air-gap as followings :

The direct axis component of armature m.m.f. at any point x from the centre pole along the machine length, assuming unity power factor is given as [5];

$$F_{od} = \hat{F}_a . \cos\left(\frac{\pi x}{\tau_p}\right) \qquad 0 \le x \le \tau_p \qquad (19)$$

whereas the flux enters the pole equal to the flux exits from it, therefore the total flux in the centre air-gap within the pole width must be zero hence ;

$$d\phi = 0 = \left(\mu_o . \frac{w_i}{g}\right) \int_{-l_{id}/2}^{+l_{id}/2} \left(\hat{F}_a . \cos\left(\frac{\pi x}{\tau_p}\right) - F_{od}\right) . dx \qquad (20)$$

then ,

$$F_{oa} = \hat{F}_a . \frac{\tau_p}{\pi . l_{id}/2} . \sin\left(\frac{\pi}{2} . \frac{l_{id}}{\tau_p}\right) \qquad (21)$$

The flux under the outer-gap is uniform distributed , this confirmed that under unsaturated condition the pole surface may considered as an equipotential surface. Assuming that there is no leakage between the adjacent poles , so the pole potential can be found easily by equating the flux crossing the centre gap to that crossing the outer-gap .

$$\phi_{centre\text{-}gap} = \phi_{outer\text{-}gap}$$

$$(F_{od} - F_p) . S_1 = F_p . S_2$$

$$\left[\hat{F}_a . \frac{2}{\pi} . \frac{\tau_p}{l_{id}} . \sin\left(\frac{\pi}{2} . \frac{l_{id}}{\tau_p}\right) - F_p\right] . S_1 = F_p . S_2 \qquad (22)$$

When the above equation is solved for $F_p$ , the fundamental component of the centre limb air-gap flux density and then the pole flux can be obtained :

$$\phi_d = C_d \cdot \frac{6.(Z_a.q.K_w).\mu_o.w_i.\tau_p.I}{\sqrt{2}.\pi^2 g} \qquad (23)$$

Where ;

$$C_d = \frac{l_{id}}{\tau_p} - \frac{1}{\pi}\sin\left(\frac{\pi}{2}.\frac{l_{id}}{\tau_p}\right) - \frac{8\tau_p}{\pi^2.l_{id}(1+(l_2w_2/l_{id}w_i)}.\sin^2\left(\frac{\pi}{2}.\frac{l_{id}}{\tau_p}\right)$$

Equating the expressions for the induced emf $E_{ad}$ and the air-gap direct reactance voltage drop $I_d.X_d$ , the armature d-axis inductance can be obtained :

$$L_{ad}.I = \frac{2.(Z_a.q.K_w)}{\sqrt{2}} \cdot p \cdot \phi_d \qquad (24)$$

$$L_{ad} = C_d \cdot \frac{6.(Z_a.q.K_w)^2.\mu_o.w_i.\tau_p.p}{\pi^2 g} \qquad (25)$$

### 3.4. Thrust and Attractive Force :

By means of conventional two-axis theory the voltage matrix equation can be represented by:

$$v = r.i + L.(di/dt) + \omega.G_i \qquad (26)$$

In this expression ;

$$i = \begin{bmatrix} i_f \\ i_q \\ i_d \end{bmatrix} , \quad L = \begin{bmatrix} L_f & & M_f \\ & L_q & \\ M_f & & L_d \end{bmatrix} , \quad G = \begin{bmatrix} & & \\ -M_f & & -L_{ad} \\ & +L_{aq} & \end{bmatrix}$$

$L_d$ , $L_q$ and $L_f$ include leakage components , i.e. ,

$L_d = L_{ld} + L_{ad}$ etc. Equation (26) can be written as ;

$$i^T.v = i^T.R.i + \frac{d}{dt}.(i^T.L.i) + \omega.i^T.G.i$$

Where, $i^T$ indicates the transpose of i , so that each term of the machine power balance can be identified. Equating the converted power to the mechanical power output gives ;

echanical power output = $\omega . [ M_f . i_f . i_q + (L_{ad} - L_{aq}) . i_d . i_q ]$

n terms of steady-state quantities ;

$i_f = I_f$ , $i_d = \sqrt{3} . I . \cos \delta_i$ , $i_q = \sqrt{3} . I . \sin \delta_i$ ,

$M_{af} = M_f / \sqrt{3}$ , periphery speed = $\tau_p . \omega / \pi$ , so that ;

$$\text{The Torque} = 3 . M_{af} . I . I_f . \sin \delta_i + \frac{3}{2} . (L_{ad} - L_{aq}) . I^2 . \sin 2\delta_i \qquad (27)$$

The thrust force under constant current conditions may given by ;

$$F_T = \frac{3\pi}{\tau_p} . M_{af} . I_f . I . \sin \delta + \frac{3\pi}{2\tau_p} . (L_{ad} - L_{aq}) . I^2 . \sin 2\delta_i \qquad (28)$$

The calculated thrust force is shown in Fig.(3). A consideration f the air-gap stored energy leads to the following attraction force $F_N$ where ;

$$F_N = \frac{\partial}{\partial g} (\text{stored energy}) = \frac{\partial}{\partial g} (i^T . L . i)$$

$$= \frac{\partial}{\partial g} [ \frac{1}{2} L_f . i_f^2 + \frac{1}{2} L_q . i_q^2 + \frac{1}{2} L_d . i_d^2 + M_f . i_d . i_f ]$$

valuating this expression gives ;

$$F_N = \frac{L_f . I_f^2}{2g} + \frac{3I^2 (L_{ad} + L_{aq})}{4g} + \frac{3I^2 (L_{ad} - L_{aq})}{4g} \cos 2\delta_i + \frac{3M_{af} . I_f . I}{g} \cos \delta_i \qquad (29)$$

Since the leakage inductance are independent of g . Equation (29) shows that there are two normal force components that are independent of torque angle ($\delta_i$) and two variable force components. The calculated normal force is shown in Fig.(4). The larger of these varies as (cos $\delta_i$) and is due to the interaction between the armature and field current distributions.

## 4. PROTOTYPE MOTOR AND EXPERIMENTAL RESULTS :

The prototype motor is made of mild steel sections with a laminated and wound centre core. The D.C. coil is positioned under the armature winding in the centre core limb. The armature windings are 3-phase with 2-slot/pole/phase and double layer winding. The poles are made of solid mild steel and have T-shape. The D.C. coils are excited from the D.C. supply and the induced e.m.f. per phase is measured in AC windings using the measured average value of the flux at pole pitch , see Fig.(5). It can be seen from Fig.(5) that, the experimental measurements of E.M.F. is quite close to theoretical E.M.F. when the effect of magnetic flux-fringing at the pole edges is considered. The prototype motor has the following data :-

| | |
|---|---|
| centre limb width $w_i$ | = 100 mm |
| pole depth | = 20 mm |
| distance between the centre limb and the outer side limb | = 115 mm |
| overall width | = 400 mm |
| air-gap depth (g) | = 20 mm |
| pole width $l_i$ at centre limb | = 80 mm |
| pole width $l_z$ at out side core limb | = 120 mm |
| pole pitch $\tau_p$ | = 180 mm |
| number of poles | = 6 |
| stator back iron thickness | = 25 mm |
| stator stack height | = 60 mm |
| number of turns of D.C. field windings $N_f$ | = 200 |
| number of turns of armature A.C. windings per phase $N_{ph}$ | = 488 |

## CONCLUSION :

In this paper, relations determining the air-gap reluctance of E- core linear synchronous motor have been taking into consideration the effect of the magnetic field fringing in the air-gap regions. In these relations, the concept of "effective pole-area" and "effective pole width" are introduced to enable more precise and quick calculations of the machine parameters.

As the analysis reveals, the effect of magnetic field fringing results in increasing the geometrical pole-area by a fictitious amount ; reducing thereby the air-gap reluctance. The corresponding reduction has naturally its effect on the machine parameters and, inturn, on the machine performance.

The laboratory measurments, carried out on the prototype motor, show that the induced E.M.F. in the armature windings due to the main excitation has a good correlation with that theoretically investigated taking into consideration the magneti flux fringing at pole edges.

The presented analysis and suggested concepts give a precise, short cut tool in the machine designer hand.

## LIST OF SYMBOLS :

$A_{ieff}$ : = Effective pole area under the centre limb.

$A_{2eff}$ : = Effective pole area under the outer limb.

$\hat{B}_{if}$ : = Centre air-gap flux density.

$F_a$ : = The peak value of resultant armature m.m.f. distribution.

$F_f$ : = Field m.m.f.

$F_p$ : = Pole magnetic potential.

$g$ : = Air-gap length at the pole centre.

$g'$ : = effective air-gap length inclusive Carter's coefficient.

$h$ : = pole depth.

$I$ : = The rms armature current.

$I_f$ : = Field current.

$K_w$ : = Fundamental winding factor.

$l_1$ : = Pole width under centre core limb.

$l_2'$ : = Pole width under outside core limb.

$l_{id}$ : = Effective pole width under centre core limb in d-axis position.
$l_{iq}$ : = Effective pole width under centre core limb in q-axis position.
$l_2$ : = Effective pole width under outside core limb.
$L_f$ : = Field winding self induction exclusive leakage component.
$L_{ad}$ : =Armature d-axis self inductance exclusive leakage component.
$L_{aq}$ : =Armature q-axis self inductance exclusive leakage component.
p : = Number of pole pairs.
q : = Slots/pole/phase.
s : = Slot width.
$S_1$ : = Centre air-gap permeance.
$S_2$ : = Outer air-gap permeance.
$w_1$ : = Centre core limb width.
$w_2$ : = Outside core limb width.
$Z_a$ : = Number of armature conductors per slot.
$Z_f$ : = Number of field conductors.
$\tau_p$ : = Pole pitch.
$\mu_o$ : = Permeability of free space.
$\delta_i$ : = Torque angle.
$\phi_1$ : = Centre air-gap flux.
$\phi_2$ : = Outer air-gap flux.

## REFERENCES

1. Levi, E. " High speed iron synchronous operating linear motor" I.E.E Conference publication on linear electric machines No 120, Oct. 1974.

2. Wiseman, R.W. " Graphical determination of magnetic fields " Trans A.I.E.E Vol 4, No. 2, pp 141-154 feb. 1972.

3. Eastham, J.F " Iron cored linear synchronous machines " Electronic and power IEE Vol 23, 1977 pp 239, 242.

4. Eastham, J. F. and Balchin, M. J. " Characteristic of heteropolar linear synchronous machines with passive secondary " IEE Vol 2, No. 6 Dec. 1979 pp 213-218.

5. Liwschitz Garik and Whipple, C.C. " Electric Machinery " Vol. 2, Van. Nostrand.

6. EL-Drieny , S. A. "Analysis of claw pole transverse flux inductor motor by means of magnetic equivalent circuit", Mansoura Engineering Journal , Vol. 12, No. 2, Dec. 1987.

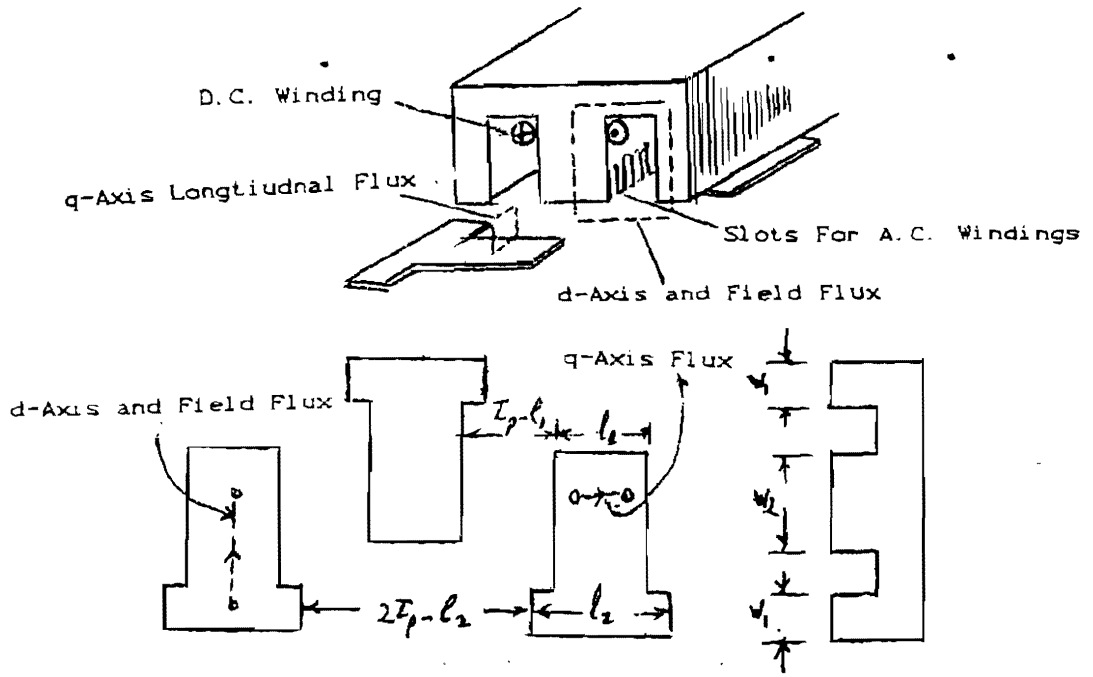


Fig.(1): E-core Transverse Flux Hetropolar Linear Synchronous Motor and Magnetic Circuit Dimensions.

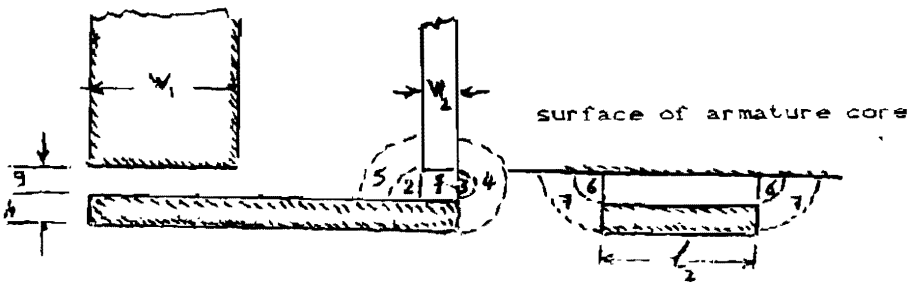


Fig.(2a) : Division of side air-gap into component flux paths.

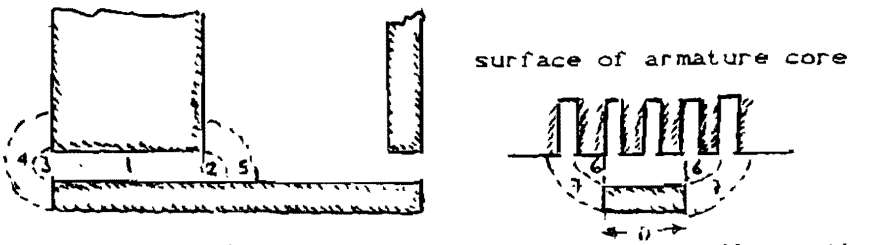


Fig.(2b) : Division of centre air-gap into component flux paths.

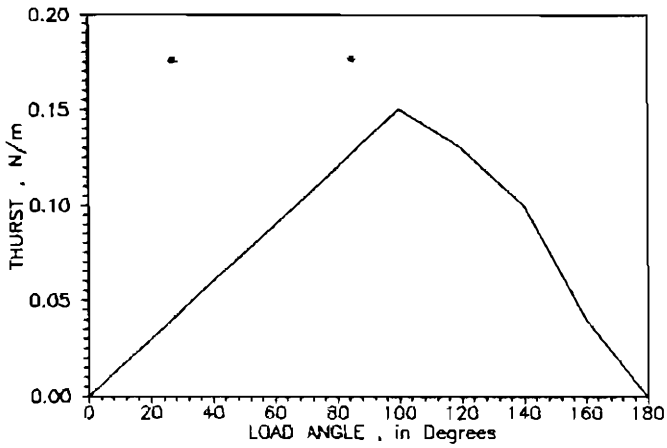


Fig.(3) : Thrust force versus load angle.

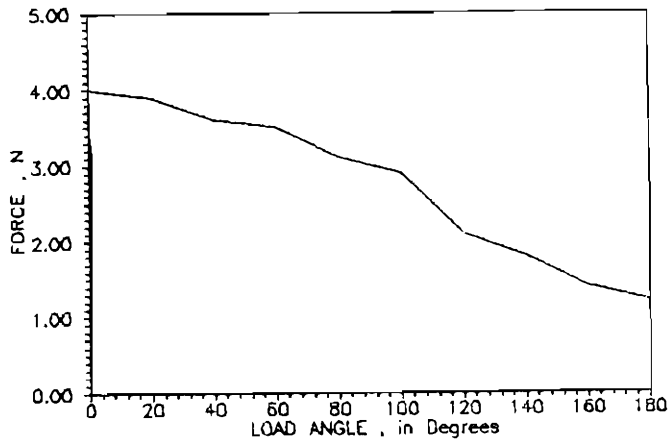


Fig.(4) : Normal force versus load angle.

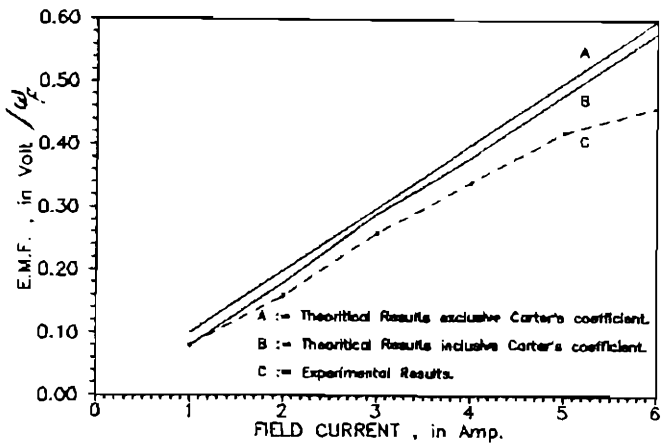


Fig.(5): Induced EMF per Phase per Angular Frequency in Armature Winding Versus Field Current.